

# Restoring coherence via aperiodic drives in a many-body quantum system

Bhaskar Mukherjee<sup>1</sup>, Arnab Sen<sup>1</sup>, Diptiman Sen<sup>2</sup>, and K. Sengupta<sup>1</sup>

<sup>1</sup>*School of Physical Sciences, Indian Association for the Cultivation of Science, Kolkata 700032, India*

<sup>2</sup>*Centre for High Energy Physics and Department of Physics,  
Indian Institute of Science, Bengaluru 560012, India*

(Dated: January 16, 2022)

We study the unitary dynamics of randomly or quasi-periodically driven tilted Bose-Hubbard (tBH) model in one dimension deep inside its Mott phase starting from a  $\mathbb{Z}_2$  symmetry-broken state. The randomness is implemented via a telegraph noise protocol in the drive period while the quasi-periodic drive is chosen to correspond to a Thue-Morse sequence. The periodically driven tBH model (with a square pulse protocol characterized by a time period  $T$ ) is known to exhibit transitions from dynamical regimes with long-time coherent oscillations to those with rapid thermalization. Here we show that starting from a regime where the periodic drive leads to rapid thermalization, a random drive, which consists of a random sequence of square pulses with period  $T + \alpha dT$ , where  $\alpha = \pm 1$  is a random number and  $dT$  is the amplitude of the noise, restores long-time coherent oscillations for special values of  $dT$ . A similar phenomenon can be seen for a quasi-periodic drive following a Thue-Morse sequence where such coherent behavior is shown to occur for a larger number of points in the  $(T, dT)$  plane due to the additional structure of the drive protocol. We chart out the dynamics of the system in the presence of such aperiodic drives, provide a qualitative analytical understanding of this phenomenon, point out the role of quantum scars behind it, and discuss experiments which can test our theory.

PACS numbers: 03.75.Lm, 05.30.Jp, 05.30.Rt

## I. INTRODUCTION

It is well-known that the bulk energy spectrum of any non-integrable many-body quantum system satisfies the eigenstate thermalization hypothesis (ETH)<sup>1–4</sup>. ETH provides a natural explanation of eventual thermalization starting from a generic non-equilibrium many-body quantum state. One of the consequence of ETH is the decay of coherent quantum oscillations in the expectation value of a generic local operator during its evolution as the system reaches a steady state<sup>5,6</sup>; such a decay is characterized by a system-dependent timescale,  $\tau_{th}$ , which is identified as the thermalization time. The divergence of the thermalization time leading to failure of ETH is seen in many-body localized systems where strong disorder leads to non-ergodicity<sup>7</sup>. Another weaker violation of ETH occurs in certain disorder-free systems due to presence of special energy eigenstates, dubbed as many-body quantum scars, in the spectrum of the bulk eigenstates of these system<sup>8–11</sup>. The consequence of presence of such states in the eigenstates of the Hamiltonian describing a Rydberg chain was experimentally verified via observation of long-time coherence oscillation of Rydberg excitations<sup>9</sup>. It was noted that such long-time oscillations, which occurs only if the starting state is  $|\mathbb{Z}_2\rangle$  (a state with one Rydberg excitation on every alternate site), could not be explained within the framework of ETH<sup>10,11</sup>. Instead, their presence occurs due to the existence of quantum scars which are states with finite energy density but sub-thermal half-chain entanglement:  $S_{L/2} \sim \ln L$  where  $L$  refers to the total number of sites in the chain. These states have large and finite overlap with  $|\mathbb{Z}_2\rangle$  and form an almost closed subspace in the system's Hilbert space. The evolution of the system, starting from

the  $|\mathbb{Z}_2\rangle$  state, therefore occurs within this almost closed subspace leading to breakdown of ergodicity and failure of ETH.

More recently, the fate of such scar-induced coherent oscillations were studied in the context of a periodically driven Rydberg chain<sup>12</sup>. It was shown that for high drive frequencies where the properties of the system can be understood in terms of a Floquet Hamiltonian  $H_F$ <sup>13</sup> computed using Magnus expansion<sup>14</sup>, the bulk eigenstates of  $H_F$  host scars whose presence lead to long-time coherent oscillations in the density-density correlation function of the Rydberg atoms. In contrast, at low frequencies,  $H_F$  do not host scars and the correlation function shows expected thermalization consistent with ETH prediction. In between, at intermediate drive frequencies, the system undergoes several reentrant transitions between thermal and coherent regimes. The reason for such transition could be analytically, albeit qualitatively, understood by noting that a special class of local terms in  $H_F$ , which are responsible for hosting scars in its eigenspectrum, have vanishing amplitude at special drive frequencies. Near these drive frequencies, the system crosses over from coherent to thermal behavior. The density-density correlator displays increasingly shorter  $\tau_{th}$  as these special frequencies are approached. The fastest thermalization occurs in the vicinity of these special frequencies where coherent oscillations are almost absent<sup>12</sup>.

In this work, we study the driven tilted Bose-Hubbard model (tBH) in the presence of random and quasiperiodic drives. The model Hamiltonian we use for such a study involves a representation of this model in terms of Ising

spins<sup>12,15</sup> and is given by

$$H_0 = \sum_j \left( -w\tilde{\sigma}_j^x + \frac{\lambda}{2}\sigma_j^z \right) \quad (1)$$

where  $\sigma_j^\alpha$  for  $\alpha = x, y, z$  denote Pauli spin matrices on site  $j$  of the chain,  $\tilde{\sigma}_j^\alpha = P_{j-1}\sigma_j^\alpha P_{j+1}$ ,  $P_j = (1 - \sigma_j^z)/2$  is a projection operator which projects to the  $|\downarrow\rangle$  state, and  $w$  and  $\lambda$  denote strength of the effective transverse and longitudinal field terms of the spin model. Furthermore, there is an additional constraint that the spins on any two neighboring sites cannot simultaneously be  $|\uparrow, \uparrow\rangle$ .

In what follows, we shall always be in the regime  $w/|\lambda| \ll 1$  and drive  $\lambda$  according to some given protocol keeping  $w$  fixed. More specifically, in this work, we shall be studying two drive protocols. The first involves a random sequences of square pulses with period  $T_\pm = T + \alpha dT$ , where  $\alpha = \pm 1$  is a random number and  $dT$  is the strength of the noise. The second protocol involve a quasiperiodic drive which follows the Thue-Morse sequence for which the sequence of numbers  $\{\alpha_i\}$ , rather than being random, satisfies

$$\{\alpha_{2n}\} = \{\alpha_n\}, \quad \{\alpha_{2n+1}\} = -\{\alpha_n\} \quad (2)$$

with  $\alpha_0 = -1$ <sup>16,17</sup>. The drive period for the  $n^{\text{th}}$  square pulse following the Thue-Morse protocol is then given by  $T_n = T + \alpha_n dT$ .

The central results that we obtain from such a study are as follows. First, starting from the initial state  $|\psi_0\rangle = (|\mathbb{Z}_2\rangle + |\bar{\mathbb{Z}}_2\rangle)/\sqrt{2}$  (where  $|\bar{\mathbb{Z}}_2\rangle$  is the time-reversed counterpart of  $|\mathbb{Z}_2\rangle$  and  $|\mathbb{Z}_2\rangle = |\uparrow\downarrow\uparrow\dots\rangle$ ), for the case of random protocol, we show that the presence of the telegraphic noise with specific noise strength  $dT$  may restore coherent oscillations of the spin correlation functions even when such correlators shows ETH predicted thermalization in the absence of noise. We demonstrate this by exact numerics on finite sized Rydberg chains with length  $L \leq 26$ . Second, using the fact that  $w/|\lambda(t)| \ll 1$  at all times, we provide an analytic explanation of this phenomenon. Our results allow us to provide a phase diagram as a function of  $dT$  and  $T$  which indicates the specific values of  $dT$  and  $T$  at which we expect such coherent behavior; these results agree qualitatively with the prediction of exact numerics. Moreover, our analysis elucidate the role of quantum scars behind this phenomenon. Third, we demonstrate the presence of coherence restoration for dynamics using Thue-Morse sequence at specific values of  $dT$  and provide a semi-analytic explanation for their occurrence. Finally, we discuss experiments involving ultracold Rydberg chain which can test our theory.

The plan of the paper is as follows. In Sec. II, we discuss the model Hamiltonian and its relation to the Hamiltonian governing the dynamics of 1D Rydberg atoms. This is followed by Secs. III and IV where we present our results on random and quasiperiodic drive protocols. Finally, we chart out our main results, discuss experiments which can be used to verify them, and conclude in Sec. V.

## II. MODELS

In this section, we chart out the model used in the present study and its relation to Hamiltonian describing atoms in a ultracold Rydberg chain. We start with the tilted Bose-Hubbard model given by

$$H = -w_0 \sum_{\langle ij \rangle} (b_i^\dagger b_j + \text{h.c.}) - \sum_i (\mu_0 + E_1 i) n_i^b + \sum_i \frac{U}{2} n_i^b (n_i^b - 1) \quad (3)$$

where  $b_i$  ( $b_i^\dagger$ ) denotes the boson annihilation (creation) operator on site  $i$  of a 1D chain,  $n_i^b = b_i^\dagger b_i$  is the number operator for bosons,  $E_1$  denotes the effective electric field for the bosons which controls the magnitude of the tilt,  $\mu_0$  is the boson chemical potential,  $w_0$  is the amplitude for nearest-neighbor hopping, and  $U$  is the on-site interaction strength.

It is well-known that the effective low-energy description of these model can be achieved in terms of dipoles living on a link  $\ell$  between two consecutive lattice sites  $j$  and  $j'$ . The creation operator for these dipoles can be written as  $d_\ell^\dagger = b_j^\dagger b_{j-1} / \sqrt{n_0(n_0 + 1)}$ , where  $n_0$  is the ground state occupation of the parent Mott state without the tilt. In terms of these dipoles the effective low-energy Hamiltonian can be written as<sup>15</sup>

$$H_d = \sum_\ell \left( -w(d_\ell + d_\ell^\dagger) + \lambda n_\ell^d \right) \quad (4)$$

where  $w = w_0 \sqrt{n_0(n_0 + 1)}$  is the amplitude for spontaneous creation and annihilation of dipoles,  $\lambda = (U - E_1)$  is the dipole chemical potential, and  $n_\ell^d = d_\ell^\dagger d_\ell$  is the dipole number operator. The Hamiltonian  $H_d$  is to be supplemented by two constraint conditions that make it non-integrable:  $n_\ell^d \leq 1$  and  $n_\ell^d n_{\ell+1}^d = 0$ . The first ensures that the maximum number of dipoles on any link is unity and the second guarantees that there are no states with two dipoles on neighboring links. For large positive  $\lambda/w$ , the ground state of the model consists of a dipole vacuum while for large negative  $\lambda/w$ , it is a  $\mathbb{Z}_2$  symmetry broken state with maximal number of dipoles which we denote as  $|\mathbb{Z}_2\rangle$ . These two states are separated by a quantum phase transition at  $\lambda/w = -1.31 \sqrt{n_0(n_0 + 1)}$  which belongs to the Ising universality class. The non-equilibrium dynamics of the model, starting from the dipole vacuum or  $|\mathbb{Z}_2\rangle$  has been studied for quench, ramp and periodic protocols<sup>18</sup>. The model has also been experimentally realized using ultracold boson chains<sup>19</sup>.

In what follows, we shall use a spin representation of this dipole model which allows us to implement the constraint in a easier manner. To this end, we use the transformation  $\sigma_\ell^{x[y]} = [i](d_\ell + [-]d_\ell^\dagger)$  and  $\sigma_\ell^z = 2n_\ell^d - 1$ . In terms of the spin variables, one obtains

$$H_s = \sum_\ell (-w\sigma_\ell^x + \lambda\sigma_\ell^z/2) \quad (5)$$

with the constraint  $(1+\sigma_\ell^z)(1+\sigma_{\ell+1}^z) = 0$ . It was noted in Ref. 11 that this constraint condition could be implemented by a local projection operator  $P_\ell = (1 - \sigma_\ell^z)/2$  which enables one to equate  $H_s$  to  $H_0$ . For  $\lambda = 0$ ,  $H_0$  only contains a single term and has been referred to as the PXP model<sup>10,11</sup>. It is well-known that for  $\lambda = 0$ , the eigenspectrum of  $H_0$  hosts quantum scars and lead to long time coherent oscillation of  $O_{\ell_1\ell_2} = \langle \sigma_{\ell_1}^z \sigma_{\ell_1+\ell_2}^z \rangle$ <sup>9</sup>.

Such a long-time coherent oscillatory behavior of the spin correlator was experimentally verified in a Rydberg chain. The effective low-energy Hamiltonian for these Rydberg atoms can be written as<sup>9</sup>

$$H_{\text{Ryd}} = \sum_i (\Omega \sigma_i^x + \Delta n_i) + \sum_{ij} V_{ij} n_i n_j \quad (6)$$

where  $n_i \leq 1$  is the number of Rydberg atoms on site  $i$ ,  $\Delta$  denotes the detuning parameter used to facilitate a Rydberg excitation,  $V_{ij} \sim 1/|i-j|^3$  is the interaction between them,  $\sigma_x^i = |R_i\rangle\langle G_i| + \text{h.c.}$  describes coupling between atoms in the Rydberg excited ( $|R_i\rangle$ ) and ground ( $|G_i\rangle$ ) states. We note that experiments on these system can tune  $V_{ij}$  such that  $V_{ii+1} \gg \Delta, \Omega \gg V_{ii+2}$ <sup>9</sup>; in this case, the interaction acts as a constraint of not having two Rydberg excitations on neighboring sites. In this regime  $H_{\text{Ryd}}$  can be directly mapped to  $H_0$  with  $\Omega \rightarrow -w$ ,  $n_i \rightarrow (1 + \sigma_\ell^z)/2$ , and  $\Delta \rightarrow \lambda$ .

Before ending this section, we note that the periodic dynamics of  $H_0$  has also been studied recently using a square pulse protocol which drives  $\lambda(t)$  between  $\lambda$  and  $-\lambda$  in the regime  $w/\lambda \ll 1$ <sup>12</sup>. In particular, the stroboscopic evolution of  $O_{22}$  as a function of the drive cycle  $n$  for several frequencies starting from the  $|\mathbb{Z}_2\rangle$  state has been shown to display long-term coherent oscillations in the high drive frequency regime. This behavior has been tied to the presence of scars in the Floquet Hamiltonian of the driven system. At low frequencies, scars were absent and the system displayed thermalization consistent with ETH. In between, at moderate drive frequencies,  $O_{22}$  shows several reentrant transitions between thermal and coherent behavior. In what follows, we are going to perform a similar study for  $H_0$  in the presence of random and quasiperiodic drive protocols.

### III. RANDOM DRIVE PROTOCOL

In this section, we shall address the dynamics of the system described by  $H_s$  (Eq. 5) in the presence of a random sequence of square pulses which makes the parameter  $\lambda$  time dependent. In this work, we shall be interested in the regime where  $w \ll |\lambda(t)|$  throughout the drive cycle. The randomness corresponds to a telegraphic noise in the drive protocol leading to a time period of  $T_\pm = T + \alpha dT$ , where  $\alpha = \pm 1$  is a random number and  $dT$  denotes the strength of the noise. Under such a drive  $\lambda(t) = +(-)\lambda$  for  $t > (<)T_\pm/2$ .

To understand the effect of such a random drive, we first note that in the absence of randomness ( $dT = 0$ ), the

dynamics of  $H_s$ , for  $w \ll \lambda$ , has been studied in Ref. 12. It was found that to  $O(w/\lambda)$ , the Floquet Hamiltonian of the system is given by

$$H_F = -w \frac{\sin(\gamma)}{\gamma} \sum_j (\cos(\gamma) \tilde{\sigma}_j^x + \sin(\gamma) \tilde{\sigma}_j^y) + \dots \quad (7)$$

where  $\gamma = \lambda T/(4\hbar)$ , the ellipsis corresponds to  $O(w^3)$  and higher order terms whose analytical form is unknown, and  $T = 2\pi/\omega_D$  is the drive period. The corresponding unitary evolution operator is given by  $U = \exp[-iH_F T/\hbar]$ . It was found that the  $O(w)$  term constitutes a renormalized PXP Hamiltonian<sup>12</sup> which vanishes for  $\gamma = n\pi$ . At these points, the Floquet Hamiltonian consists of  $O(w^3)$  (and higher powers of  $w$ ) terms which have different structure compared to PXP Hamiltonian. For  $\gamma \neq n\pi$ , the  $O(w)$  term has the most dominant contribution in  $H_F$ . Moreover, the form of these  $O(w)$  terms ensures that when they are dominant, the Floquet spectrum hosts scars which lead to long-time coherent dynamics. In contrast, for  $\gamma = n\pi$ , eigenstates of the Floquet Hamiltonian do not host scars and the system exhibits thermalization consistent with ETH.

For random drives it is easy to see that for  $T = T_\pm$ , the unitary evolution operators controlling the evolution are given by

$$U_\pm = e^{-iH_F^\pm T_\pm}, \quad H_F^\pm = H_F(\gamma \rightarrow \gamma_\pm) \quad (8)$$

where  $\gamma_\pm = \lambda T_\pm/(4\hbar) = \gamma \pm d\gamma$ , and  $d\gamma = \lambda dT/(4\hbar)$ . Thus for a random protocol, the wavefunction after  $n$  cycles of the drive would be

$$|\psi_n\rangle = U_- U_- U_+ \dots U_+ |\psi_0\rangle = \mathcal{U} |\psi_0\rangle \quad (9)$$

where  $|\psi_n\rangle$  denotes the wavefunction after  $n$  drive cycles starting from the initial state  $|\psi_0\rangle$ , and  $U_+$  and  $U_-$  occurs randomly with equal probability in the string of evolution operators represented by  $\mathcal{U}$  in Eq. 9.

In the presence of such a drive, the effect of randomness manifests itself through the action of the commutator  $[U_+, U_-]$  on the state. This can be easily seen by noting that the Floquet eigenvectors corresponding to  $U_\pm$  changes only when it is operated on by a subsequent  $U_\mp$  in the random string in Eq. 9. This change occurs since eigenvectors of  $U_+$  and  $U_-$  are different; it vanishes if  $U_+$  and  $U_-$  commute. Such commutation of  $U_+$  and  $U_-$  clearly occurs for  $dT = 0$  since it amounts to absence of randomness. However, in the  $w \ll |\lambda(t)|$  limit, the leading terms of these commutators also vanish at special values of  $dT/T$ . To see this we compute  $\mathcal{C} = [U_+, U_-]$ . Using Eqs. 7 and 8 we find

$$\begin{aligned} \mathcal{C} &= \mathcal{C}_0 + \dots \\ &= \left(\frac{4w}{\lambda}\right)^2 \sin(2d\gamma) \sin(\gamma + d\gamma) \sin(\gamma - d\gamma) \\ &\quad \times \sum_{j,j'} [\tilde{\sigma}_j^y, \tilde{\sigma}_{j'}^x] + \dots \end{aligned} \quad (10)$$

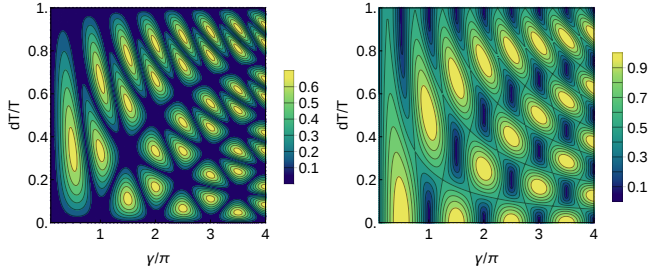


FIG. 1: Left Panel: Plot of  $\|\mathcal{C}_0\|(\lambda/4w)^2$  as a function of  $\gamma$  and  $dT/T$  showing dips at  $dT/T = k\pi/2$  and  $k\pi + \gamma$ . Right: Plot of  $\|H_F^{\text{av}}\|/w$  as a function of  $\gamma$  and  $dT/T$ .

where the expression is valid for  $w/\lambda \ll 1$  and the ellipsis beyond  $\mathcal{C}_0$  indicate higher order terms in  $w/\lambda$ . We note that if the norm of the commutator vanishes, it is possible to rearrange  $U_-$  and  $U_+$  in Eq. 9 in pairs. Since in the random string of evolution operators in Eq. 9, the occurrence of  $U_+$  and  $U_-$  are equally likely, for large enough  $n$ , the dynamics could have been described by an average Floquet Hamiltonian:  $|\psi(t)\rangle \simeq \exp[-iH_F^{\text{av}}nT]|\psi_0\rangle$ , where

$$\begin{aligned} H_F^{\text{av}} &= (H_+T_+ + H_-T_-)/(2T) + \dots \\ &= \frac{w}{\gamma} \sum_j [c_1(T)\tilde{\sigma}_j^x + c_2(T)\tilde{\sigma}_j^y] + \dots \\ c_1(T) &= \sin(2[\gamma + d\gamma]) + \sin(2[\gamma - d\gamma]) \\ c_2(T) &= 2 - \cos(2[\gamma + d\gamma]) - \cos(2[\gamma - d\gamma]) \end{aligned} \quad (11)$$

where ellipsis indicate terms  $O(w^m)$  for  $m \geq 3$  which do not support scars<sup>12</sup>.

Using Eqs. 10 and 11, we can now chart out analytical conditions for having long-time coherent oscillations in the presence of the random drive. The first condition for such oscillation is sufficiently weak randomization of Floquet eigenstates which occurs when the leading term in norm of commutator  $\|\mathcal{C}_0\| = (4w/\lambda)^2 \sin(2d\gamma) \sin(\gamma + d\gamma) \sin(\gamma - d\gamma)$  vanishes. This leads to the condition

$$d\gamma = k\frac{\pi}{2} \quad \text{or} \quad d\gamma = k\pi \pm \gamma \quad (12)$$

where  $k \in \mathbb{Z}$ . We note that Eq. 12 constitutes a necessary but not sufficient condition for coherent oscillations. For such oscillations, in addition to weak enough randomization of Floquet eigenvectors, one also needs to ensure that  $H_F^{\text{av}}$  which controls the dynamics when  $\|\mathcal{C}_0\| = 0$ , hosts scars. This requires an additional constraint that the leading term in the norm of  $H_F^{\text{av}}$ ,  $\|H_F^{\text{av}}\| = w\sqrt{c_1(T)^2 + c_2(T)^2}$ , does not vanish (*i.e.*,  $c_1(T)$  and  $c_2(T)$  do not vanish simultaneously). This leads to the condition

$$d\gamma \neq k'\pi \quad \text{if} \quad \gamma = k\pi \quad (13)$$

where  $k, k' \in \mathbb{Z}$ . We note that the conditions Eq. 12 and 13 ensure that the effect of the telegraphic noise is

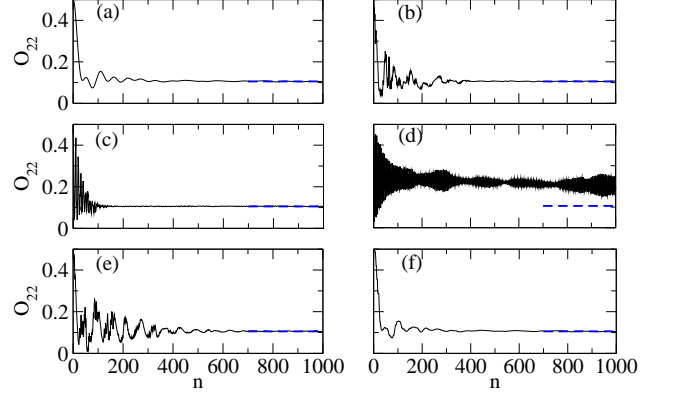


FIG. 2: Plot of  $O_{22}$  as a function of the number of drive cycle  $n$  for  $L = 26$ ,  $\omega_D = 7.75$  and  $\lambda = 15$  for (a)  $dT/T = 0$ , (b) 0.1, (c) 0.3, (d) 0.5, (e) 0.9, and (f) 1. The plot indicates clear return of coherent oscillation for  $dT/T = 0.5$ . All energies (frequencies) are scaled in units of  $w/\sqrt{2}$  ( $w/(\hbar\sqrt{2})$ ) and  $\hbar$  is set to unity. The blue dashed line in all panels corresponds to the infinite temperature ensemble value of  $O_{22}$ .

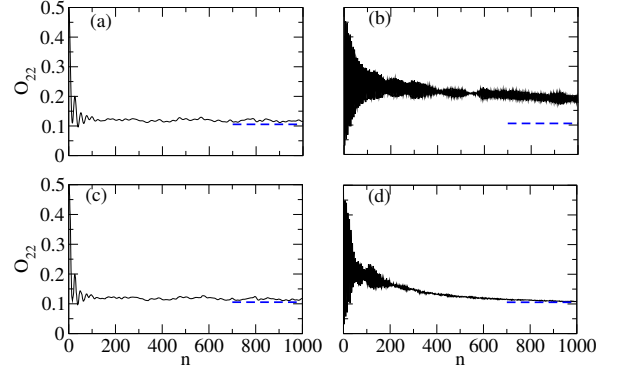


FIG. 3: Plot of  $O_{22}$  as a function of  $n$  for  $L = 26$ ,  $\omega_D = 3.9$  and  $\lambda = 15$  (a)  $dT/T = 0$ , (b) 0.25, (c) 0.5, and (d) 0.75. The coherent oscillatory behavior exhibits a much slower decay time for  $dT/T = 0.25$  than for  $dT/T = 0.75$ . All units and the definition of the blue dashed line are same as in Fig. 2.

minimal and that the dynamics is controlled by scars in the eigenspectrum of  $H_F^{\text{av}}$ . Thus these points in the parameter space of the system is likely to host coherent oscillations. These conditions are represented in Fig. 1. The left panel shows the regions in  $dT/T - \gamma$  plane where  $\|\mathcal{C}_0\| = 0$ , while the right panel indicates regions where  $\|H_F^{\text{av}}\|$  remains finite. The common points between these two regions that satisfy both these criteria are the ones where one expects restoration of coherence in the presence of noise.

To verify the restoration of coherence, we numerically



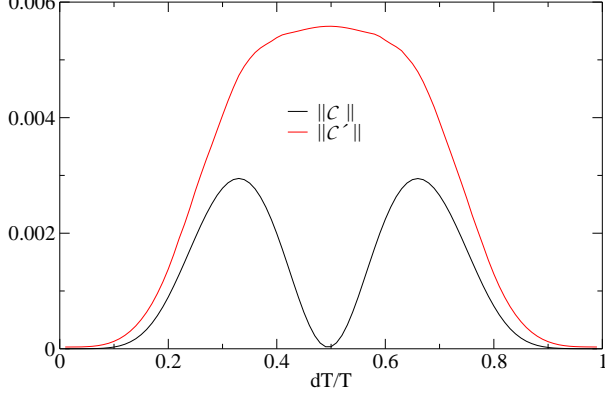


FIG. 4: Plot  $\|\mathcal{C}\|$  (black solid line) and  $\|\mathcal{C}'\|$  (red solid line) (both normalized by the square of the Hilbert space dimension) for  $L = 26$  and  $\omega_D = 7.75$  as a function of  $dT/T$  showing clear dip of  $\|\mathcal{C}\|$  at  $dT/T = 1/2$ . All units are same as in Fig. 2.

compute  $O_{\ell 2}$ . To this end, we note that both  $U_+$  and  $U_-$  can be expressed in terms of the eigenvalues  $\epsilon_p^{(1)[(2)]}$  and eigenvectors  $|p^{(1),[(2)]}\rangle$  of  $H_s^{1[2]} = H_F(+[-]\lambda)$  as

$$U_{\pm} = \sum_{p,q} e^{-i(\epsilon_q^{(1)} + \epsilon_p^{(2)})T_{\pm}/2} \mu_{pq}^{12} |p^{(2)}\rangle \langle q^{(1)}| \quad (14)$$

where  $\mu_{pq}^{12} = \langle p^{(2)} | q^{(1)} \rangle$ . These eigenvalues and eigenvectors are computed numerically using exact-diagonalization for finite-size system with  $L \leq 26$ . Using this, one can numerically compute  $O_{\ell 2}$  as

$$O_{\ell 2} = \langle \psi_0 | \mathcal{U}^\dagger \sigma_\ell^z \sigma_{\ell+2}^z \mathcal{U} | \psi_0 \rangle \quad (15)$$

We note that translational symmetry ensures that  $O_{\ell 2}$  is independent of  $\ell$ ; in what follows we shall therefore concentrate on  $O_{22}$ .

The numerical plot of  $O_{22}$ , shown in Figs. 2 and 3, supports the expectation obtained from the analytical consideration charted out earlier in the section. In Fig. 2, we plot  $O_{22}$  as a function of the number of drive cycles  $n$ , for  $\omega_D = 7.75$  (which corresponds to  $\gamma \simeq 2$ ) and for several representative values of  $dT/T$ . We note that for these systems, for  $dT = 0$ , the system shows rapid thermalization consistent with ETH as pointed out in Ref. 12. Here we find that coherent oscillations pick as we tune towards  $dT/T = 0.5$ , where  $\|\mathcal{C}_0\| = 0$  and  $\|H_F^{\text{av}}\| \neq 0$ . At  $dT/T = 0.5$ , the system exhibits long-time coherent oscillations and constitutes an example of coherence restoration by temporal disorder. To check that this is indeed the case, we plot  $\|\mathcal{C}\| = \|[U_+, U_-]\|$  and  $\|\mathcal{C}'\| = \|[U_+, U_-]\|$  (normalized by the square of the Hilbert space dimension) for  $\omega_D = 7.75$  as a function of  $dT/T$ . The plot, shown in Fig. 4, indicates a clear dip of  $\|\mathcal{C}\|$  at  $dT/T = 0.5$  where  $\|\mathcal{C}'\|$  remain finite. This

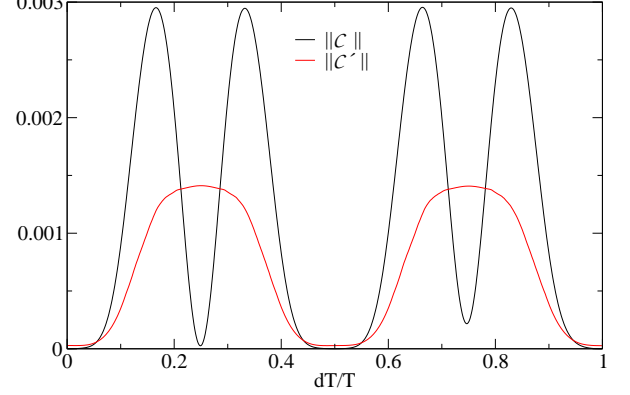


FIG. 5: Plot of  $\|\mathcal{C}\|$  (black solid line) and  $\|\mathcal{C}'\|$  (red solid line) (both normalized by the square of the Hilbert space dimension) for  $L = 26$  and  $\omega_D = 3.9$  as a function of  $dT/T$  showing clear dip of  $\|\mathcal{C}\|$  at  $dT/T = 1/4, 1/2$ , and  $3/4$ . Note that  $\|\mathcal{C}'\|$  also vanishes around  $dT/T = 1/2$  whereas it remains finite for  $dT/T = 1/4$  and  $3/4$ . All units are same as in Fig. 2.

corroborates our expectation from the earlier discussion based on analysis of  $\|\mathcal{C}_0\|$  and  $\|H_F^{\text{av}}\|$ .

A similar noise-induced restoration of coherence is seen in Fig. 3 for  $\omega_D = 3.9$  ( $\gamma \simeq 4$ ) where long-time coherent oscillations of  $O_{22}$  returns at  $dT/T = 1/4, 3/4$ . This is in accordance with prediction of Eqs. 12 and 13. Note that in this case  $\|\mathcal{C}_0\| = 0$  at  $dT/T = 0.5$ ; however  $\|H_F^{\text{av}}\|$  also vanishes at this point and  $O_{22}$  does not exhibit long-time oscillations. The analytical prediction is further verified by numerical plot of  $\|\mathcal{C}\|$  and  $\|\mathcal{C}'\|$  at  $\omega_D = 3.9$  as a function of  $dT/T$  as shown in Fig. 5. We find clear dip in  $\|\mathcal{C}\|$  at  $dT/T = 1/4, 1/2, 3/4$ . However, at  $dT/T = 1/2$ ,  $\|\mathcal{C}'\|$  also vanishes leading to absence of long-term coherent oscillations as discussed. Finally, we note that the restoration of coherence is more robust at  $dT/T = 1/4$  compared to  $dT/T = 3/4$ . This feature can be qualitatively understood as follows. We first note that the thermalization in these systems leading to destruction of coherence occurs due to action of  $\mathcal{C}$ ; thus  $\|\mathcal{C}\|$  is an indicator of the strength of this term. Next, we note that such terms lead to finite matrix elements between states within the scar subspace and states within the ETH band. This can be checked by noting that  $\mathcal{C}_0$  (the first term in Eq. 10) indeed leads to such matrix elements. Thus it is expected that the thermalization time of  $O_{22}$ ,  $\tau_{\text{th}}$ , would depends on  $\|\mathcal{C}\|$ . The expression of  $\tau_{\text{th}}$  can be estimated using Fermi's golden rule and assuming a constant density of state  $\rho_0$  for states in the thermal band to be  $\tau_{\text{th}}^{-1} \simeq (2\pi/\hbar)\rho_0\|\mathcal{C}\|^2 \sim \|\mathcal{C}\|^2$ . Thus a larger  $\|\mathcal{C}\|$  is expected to lead to shorter thermalization time and faster loss of coherence. This features is manifested in relatively shorter thermalization time of oscillations for  $dT/T = 0.75$  in Fig. 3 compared to those for  $dT/T = 0.25$ . Although  $\|\mathcal{C}_0\|$  vanishes in both case, the

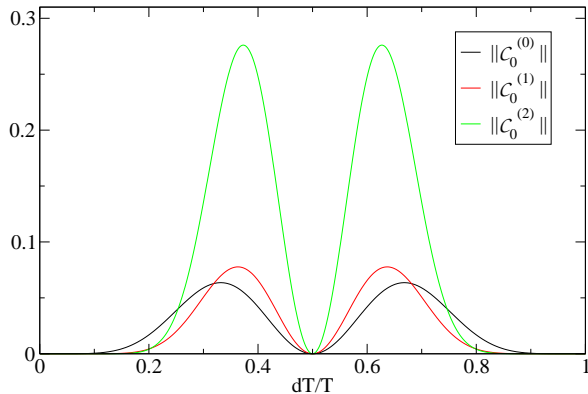


FIG. 6: Plots of  $\|\mathcal{C}_0^{(0)}\|$  (black line),  $\|\mathcal{C}_0^{(1)}\|$  (red line) and  $\|\mathcal{C}_0^{(2)}\|$  (green line) versus  $dT/T$ , for  $\omega_D = 7.5$ , and  $\lambda = 15$ . All units are same as in Fig. 2.

remaining terms lead to a larger  $\|\mathcal{C}\|$  and hence shorter thermalization time for  $dT/T = 0.75$ .

#### IV. QUASIPERIODIC DRIVE PROTOCOL

In this section, we will study the dynamics of the system when it is driven by a Thue-Morse sequence (TMS) generated by the two evolution operators  $U_+$  and  $U_-$  given in Eq. (8). The motivation for this is that a TMS generated by two non-commuting operators is known to generate unusual long-time behaviors which are quite different from those generated by a random sequence<sup>17</sup>. The TMS is generated as follows<sup>17</sup>. Defining  $A_0 = U_+$  and  $B_0 = U_-$ , we recursively define

$$A_{m+1} = B_m A_m, \quad B_{m+1} = A_m B_m, \quad (16)$$

for all  $m \geq 0$ . The wave function after  $2^n$  drives is then given by

$$|\psi_{2^n}\rangle = A_n |\psi_0\rangle. \quad (17)$$

For instance, the wave function after  $2^3 = 8$  drives is

$$|\psi_8\rangle = A_3 |\psi_0\rangle = U_- U_+ U_+ U_- U_+ U_- U_- U_+ |\psi_0\rangle. \quad (18)$$

It is clear that one can use the recursion relations in Eq. (16) to generate a sequence of  $2^n$  drives by performing only  $2n$  matrix multiplications. This enables us to study relatively easily what happens after an exponentially large number of drives.

We will now study the conditions under which the dynamics generated by Eqs. (16-17) gives long-time coherent oscillations. As discussed in Sec. III, this will happen if the evolution operators  $A_0$  and  $B_0$  commute, but  $A_1 = B_0 A_0$  is not equal to the identity operator and it

has scar states as its eigenstates. However, the recursive form of Eq. (16) implies that even if  $A_0$  and  $B_0$  do not commute, we can still obtain long-time coherent oscillations if  $A_1$  and  $B_1$  commute (since the unitary dynamics after an even number of drives can be written solely in terms of  $A_1$  and  $B_1$ ), but  $A_2 = B_1 A_1$  is not equal to the identity and it hosts scar states. Clearly, this idea can work at higher and higher levels. We thus obtain a hierarchy of possibilities for getting coherent oscillations, given by the condition that although  $A_{n-1}$  and  $B_{n-1}$  do not commute,  $A_n$  and  $B_n$  commute and  $A_{n+1} = B_n A_n$  is not equal to the identity and it hosts scars. We define the norm of the level  $n$  commutator as  $\|\mathcal{C}^{(n)}\| \equiv \|[A_n, B_n]\|$ . To demonstrate this point, we consider the  $O(w)$  approximation to  $H_F$  and write  $U_{\pm} = \exp[-iH_F^{\pm}T/\hbar]$ , where  $H_F^{\pm}$  is given by Eq. 7 with  $\gamma \rightarrow \gamma_{\pm}$ . Using these we construct the matrices  $A_1 = U_+ U_-$  and  $B_1 = U_- U_+$  and compute  $\|\mathcal{C}_0^{(1)}\|$ . A similar procedure leads to  $\|\mathcal{C}_0^{(2)}\|$ . Here, the subscript 0 in  $\mathcal{C}_0^{(n)}$  refers to the fact that only the  $O(w)$  approximation to  $H_F$  was used for the computations. Fig. 6 shows plots of  $\|\mathcal{C}_0^{(n)}\|$  versus  $dT/T$  for  $n = 0, 1$  and  $2$ , when  $\omega = 7.5$ ,  $w = 1/\sqrt{2}$ , and  $\lambda = 15$ . These norms are seen to approach zero for a range  $dT/T \leq 0.2$  and  $dT/T \geq 0.8$  implying that coherent oscillations can be expected to occur around such values. We note however that these expectations from a  $O(w)$  theory is qualitative; clearly higher order terms are expected to reduce this range to (possibly) discrete points. A more precise investigation of this behavior requires exact numerics which we now carry out.

The plot of the correlation function  $O_{22}$  as a function of  $n$  for  $\omega_D = 7.5$ ,  $w = 1$ ,  $\lambda = 15$  and several representative values of  $dT/T$  is shown in Fig. 7. The left panel shows results for the random protocol while the right panel shows that for TMS. We note that similar to the random sequence discussed in Sec. III, the TMS also leads to quick thermalization when  $\|\mathcal{C}_0^{(0)}\| \neq 0$ , and to coherent oscillation when  $\|\mathcal{C}_0^{(0)}\| = 0$  but the leading term in  $\|H_F^{\text{av}}\|/w$  is non-zero. This can be from Fig. 7(e) and (f) where both the random (Fig. 7(e)) and TMS (Fig. 7(f)) at  $dT/T = 0.5$  display coherent oscillations. However, as shown in the top panel ( $dT/T = 0.1$ ) of Fig. 7, TMS may lead to oscillatory behavior at special values of  $dT/T$  (Fig. 7(b)) even when random protocol leads to thermalization (Fig. 7(c)). In the middle panel of Fig. 7, a comparison between the behavior of  $O_{22}$  driven by random (Fig. 7(c)) and TMS (Fig. 7(d)) also indicates a much longer thermalization time for the latter. This can be understood to be a precursor to the oscillatory behavior of  $O_{22}$  for TMS at  $dT/T = 0.3$ , analogous to that found for  $dT/T = 0.1$ .

It turns out there are several such special points in the  $(T, dT)$  parameter space where the random and TMS show drastically different behaviors, namely, rapid thermalization for the random sequence but coherent oscillations for the TMS. We demonstrate four other such point in Fig. 8. For all such points, the random drive leads to

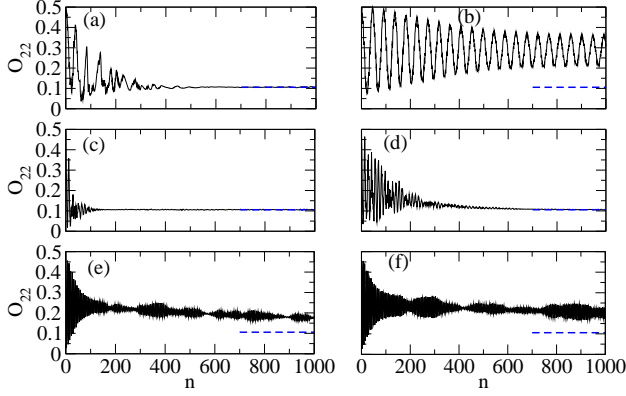


FIG. 7: Comparison of  $O_{22}$  as a function of  $n$  for random (left column) and TMS (right column) at some special points, with  $L = 26$ ,  $\omega_D = 7.5$ , and  $\lambda = 15$ . (a)-(b)  $dT/T = 0.1$ , (c)-(d)  $dT/T = 0.25$ , and (e)-(f)  $dT/T = 0.5$ . All units and the definition of the blue dashed line are same as in Fig. 2.

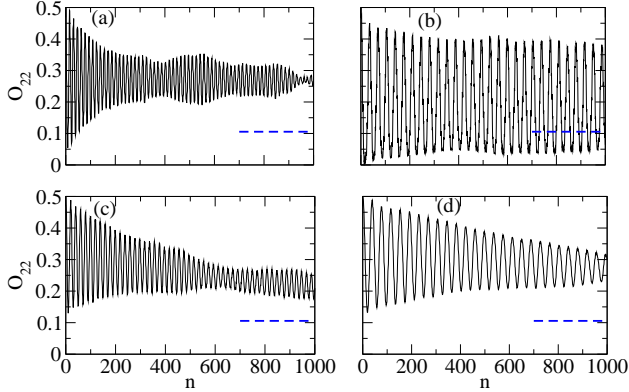


FIG. 8: Plot of  $O_{22}$  as a function of  $n$  for the TMS showing oscillatory behavior for (a)  $dT/T = 0.1$ ,  $\omega_D = 6.75$  (b)  $dT/T = 0.1$ ,  $\omega_D = 8.25$  (c)  $dT/T = 0.3$ ,  $\omega_D = 2.5$ , and (d)  $dT/T = 0.3$ ,  $\omega_D = 5$ . For all these parameter values, the random protocol shows rapid thermalization. All units and the definition of the blue dashed line are same as in Fig. 2.

rapid thermalization. The coherent behavior of  $O_{22}$  thus reflects the quasiperiodic nature of the TMS which is distinct from a totally random sequence. At these parameter values, the special form of the noise correlation in the TMS (i.e., the particular form of the sequence of  $U_+$ 's and  $U_-$ 's), although not comparable to a perfectly periodic sequence, is sufficient to preserve the memory of the initial  $|\mathbb{Z}_2\rangle$  state for a long time.

Due to the aperiodic nature of the TMS, it seems difficult to describe the special points based on an effective

many-body Floquet Hamiltonian. However, we find that it is possible to find the positions of these special points without studying the exact many-body dynamics (which is numerically difficult). We demonstrate this by studying the dynamics of a two-level system governed by the following Hamiltonian

$$H_{2 \times 2} = -w \frac{\sin \gamma}{\gamma} (\cos \gamma \sigma^x + \sin \gamma \sigma^y). \quad (19)$$

This is basically the  $O(w)$  Hamiltonian in Eq. (7) but with only one site. We now calculate  $U_{\pm}$  using this Hamiltonian and the driven wave function by acting with  $U_+$  and  $U_-$  on the initial state ( $\psi_0 = (1, 0)^T$ ) for a total of  $n_{tot}$  times following the TMS (we choose  $n_{tot} = 1000$ ). The two-component driven wave function  $\psi_n$  can be mapped to the Bloch sphere ( $\theta(n), \phi(n)$ ) using the parametrization

$$\psi(n) = (\cos(\theta/2)e^{i\phi/2}, \sin(\theta/2)e^{-i\phi/2})^T. \quad (20)$$

We find completely chaotic motion of  $\psi_n$  on the Bloch sphere for parameters which show quick thermalization to the infinite temperature ensemble in the exact many-body dynamics (see Fig. 9 (a)). On the other hand,  $\psi_n$  follows a regular trajectory on the Bloch sphere when we have coherent oscillations in the exact many-body dynamics. We find that this coherent behavior can be further categorized into *at least* three classes. For parameter values where  $\|\mathcal{C}_0^{(0)}\| = 0$  but the leading term in  $\|H_F^{av}\|/w$  is non-zero, the trajectory is just a single circle (see Fig. 9 (b)), whereas at the special points, we see either three circles (see Figs. 9 (c)-(e) or Fig. 10 (c)) or a closed curve made of intertwined ellipses (see Fig. 10(b),(d)). In fact, both the latter cases are encountered when (for example)  $dT/T$  is kept fixed at 0.1 and  $\omega_D$  is varied (see Fig. 10 (a)). In the three circle case, we further see that  $\psi_n$  for even values of  $n$  are concentrated on one circle, while  $\psi_n$  for odd values of  $n$  are concentrated on the other two circles. The one circle and the three circle cases can be understood using the recursive structure for the TMS. When  $\|\mathcal{C}_0^{(0)}\| = 0$ ,  $U_+$  and  $U_-$  commute with each other; this implies that these can be written as

$$U_+ = e^{i\alpha_+ \hat{n}_+ \cdot \vec{\sigma}}, \quad U_- = e^{i\alpha_- \hat{n}_- \cdot \vec{\sigma}}, \quad (21)$$

where the unit vectors  $\hat{n}_+$  and  $\hat{n}_-$  are identical, and  $\alpha_{\pm}$  are non-zero. Hence every term in the TMS sequence has the form given by  $\exp(if_n \hat{n}_+ \cdot \vec{\sigma})$ , where  $f_n$  is a number which depends on the number of  $U_+$ 's and  $U_-$ 's which appear in the  $n$ -th term of the TMS. The trajectory of  $|\psi_n\rangle$  therefore lies on a single circle on the Bloch sphere. At other special points like in Fig. 9 (c)-(e) and Fig. 10 (c),  $U_+$  and  $U_-$  do not commute with each other, but  $U_+U_-$  and  $U_-U_+$  approximately commute with each other, namely,  $\|\mathcal{C}_0^{(0)}\| \neq 0$  but  $\|\mathcal{C}_0^{(1)}\| \simeq 0$ . This implies that  $U_+U_-$  and  $U_-U_+$  can be written in forms similar to Eq. (21), with identical unit vectors. Hence after any even number of drives (which are given by products of a

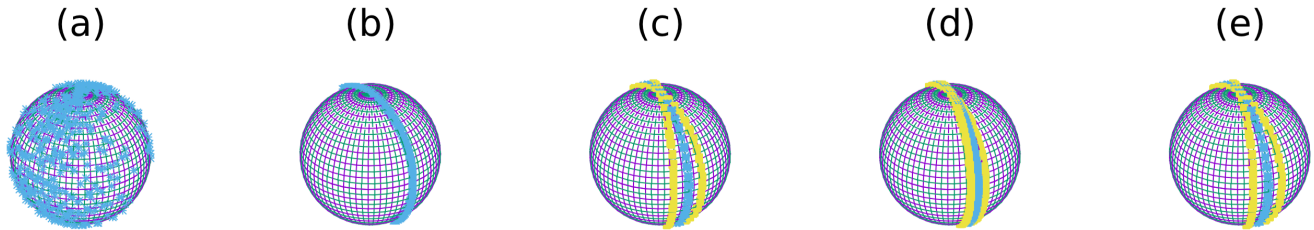


FIG. 9: Motion of  $\psi_n$  on Bloch sphere for  $\lambda = 15$ , and  $(\omega_D, dT/T) =$  (a) (7.5, 0.3), (b) (7.5, 0.5), (c) (7.5, 0.1), (d) (5.0, 0.3), (e) (2.5, 0.3). In (c)-(e) the yellow (blue) circles are for odd (even) values of  $n$ . See text for details. All units are same as in Fig. 2.

certain number of  $U_+U_-$  and  $U_-U_+$ ), we will get points which lie on a single circle on the Bloch sphere. But after an odd number of drives, we will get a point which corresponds to the single circle mentioned above multiplied by either  $U_+$  or  $U_-$  depending on which of the two ap-

pears at the last drive; these will give two different circles as  $U_+$  and  $U_-$  do not commute. Then, there are other special points where the trajectory on the Bloch sphere is not composed of a single or a three circle but a more complicated closed curve (Fig. 10 (b) and Fig. 10 (d)).

A single quantity as a function of  $\omega_D$  would be useful to see the rarity of the special points where coherent oscillations occur. We note that a regular trajectory means that the fluctuation  $\Delta_{\cos(\phi)}$  in  $\cos \phi(n)$  (where  $\phi(n)$  denotes the value of azimuthal angle  $\phi$  after  $n$  drive cycles) will be small. We define

$$\Delta_{\cos(\phi)} = \sqrt{\frac{\sum_{n=1}^{n_{tot}} (\cos \phi(n) - \cos \phi_{av})^2}{n_{tot}}}, \quad (22)$$

where  $\cos \phi_{av} = [\sum_{n=1}^{n_{tot}} \cos \phi(n)]/n_{tot}$ . We plot  $\Delta_{\cos(\phi)}$  vs  $\omega_D$  (for both random and TMS) and mark the special points (characterized by prominent dips for only the TMS) by violet circles in Fig. 11.

The above observations suggest that the coherent oscillations at the special points can be qualitatively understood based on a single site problem; hence they are only due to the interplay between the drive parameters ( $T, dT$ ) and the drive sequence (TMS in this case). Many-body effects hardly change the positions of these special points.

## V. DISCUSSION

In this work, we have studied the driven tilted Bose-Hubbard model for aperiodic drive protocols. Our results indicate that for both random and quasiperiodic drives, the presence of aperiodicity can lead to coherent behavior even when the system thermalizes in their absence. We have presented an analytical, albeit qualitative, explanation for this phenomenon and pointed out the role of quantum scars behind it.

For random drive protocols, we find that there are specific points in the  $(T, dT)$  plane, where the commutator of the evolution operators  $U_+ \equiv U(T + dT)$  and

$U_- \equiv U(T - dT)$  vanish to  $O(w^2/\lambda^2)$ . This means norm of such commutators become extremely small at these points leading to minimal decoherence due to noise. If at such points  $U_{\pm}$  supports scars in their Floquet Hamiltonian  $H_F^{\pm}$  (note that while one cannot define the Floquet Hamiltonian for the entire random string of  $U_+$  and  $U_-$ , each individual  $U_+$  and  $U_-$  have a well-defined  $H_F$ ), one sees coherent oscillations of correlation functions. We have charted out the phase diagram in the  $(T, dT)$  plane showing existence and location of such points showing that random drives can be instrumental in restoring coherence in an otherwise thermalizing system which hosts quantum scars in its Floquet spectrum.

For the quasi-periodic drive protocol, we have chosen the Thue-Morse sequence. We have shown that the inherent structure of such a drive protocol leads to several additional coherence restoring points in the  $(T, dT)$  plane where the random protocol leads to thermalizing behavior. We have plotted an approximate phase-space trajectory for such drives on the local Bloch sphere using a simplified  $2 \times 2$  local Hamiltonian. This analysis leads to four distinct class of trajectories. Three of them, namely, chaotic, single circle and three circles have a simple explanation as discussed here. However, the intertwined elliptic trajectories does not seem to yield to a simple qualitative explanation. We note here that similar complicated dynamical behavior was studied for a single spin-1/2 subjected to a Fibonacci drive sequence in Ref. 20. The generalization of this work to the Thue-Morse sequence is left for future work.

The fluctuations of the azimuthal angle of these trajectories are shown to provide a signature for coherent behavior of the many-body system. It will be useful to understand why the points at which coherence is restored in the full many-body driven problem shifts so little from



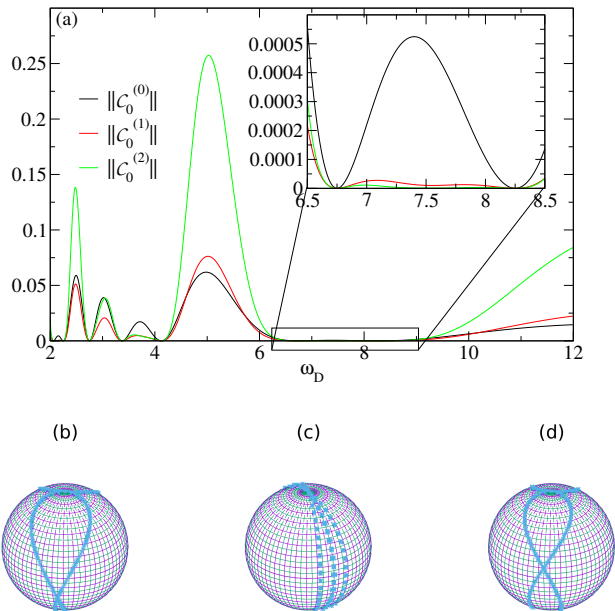


FIG. 10: (a) Plots of  $\|C_0^{(0)}\|$  (black line),  $\|C_0^{(1)}\|$  (red line) and  $\|C_0^{(2)}\|$  (green line) versus  $\omega_D$  for a fixed  $dT/T = 0.1$ , and  $\lambda = 15$ . Motion of  $\psi_n$  on Bloch sphere for  $\lambda = 15$ ,  $dT/T = 0.1$  and  $\omega_D$  equal to (b) 6.75 (c) 7.5 and (d) 8.25. All units are same as in Fig. 2.

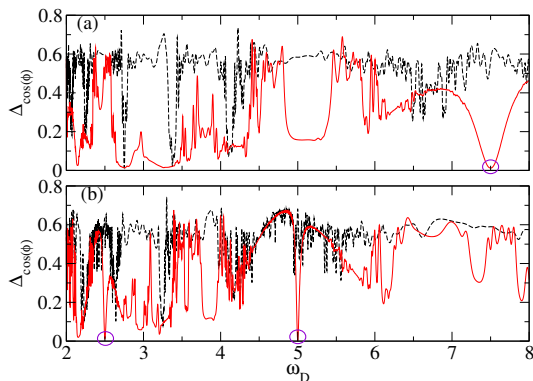


FIG. 11: Plot of  $\Delta_{\cos(\phi)}$  vs  $\omega_D$  for  $\lambda = 15$ ,  $dT/T =$  (a) 0.1 (b) 0.3. Black dashed (red solid) lines denotes the graph for random (TM) sequences. Violet circles denote the special points. All units are same as in Fig. 2.

the results of this simplified analysis. Furthermore, the mechanism and phase diagram of possible coherence revivals using other forms of quasiperiodic drive sequences, like the Fibonacci sequence<sup>21</sup>, should also be explored. We leave these issues as problems to be explored in future works.

The model we have studied is known to provide a low-energy effective description for ultracold Rydberg atoms on which quench experiments have already been performed<sup>9</sup>. Here we suggest a drive protocol where the detuning parameter is varied randomly with periodicity  $T + dT$  or  $T - dT$ . Our prediction, for example, is that for starting from the regime  $\Delta = 15$  (in units of  $\sqrt{2}\Omega$ ) and  $\omega_D = 7.75$  (in units  $\sqrt{2}\Omega/\hbar$ ) where all values  $dT < 0.5$  leads to rapid thermalization, the Rydberg excitation density and density-density correlation function will display long-time coherent oscillatory behavior for  $dT/T = 0.5$ . Richer, albeit similar, effects for coherence restoration shall also be present for a quasiperiodic (Thue-Morse) drive sequence as has been discussed here.

In conclusion, we have studied driven titled Bose-Hubbard model with aperiodic drive. We have shown that the presence of randomness or quasi-periodicity in the drive protocol may restore coherence in such a driven system. We have provided analytic explanation of our results, pointed out the role of quantum scars behind such coherent behavior, and discussed the possibility of its experimental signature in a driven ultracold Rydberg chain.

## Acknowledgments

The work of A.S. is partly supported through the Partner Group program between the Indian Association for the Cultivation of Science (Kolkata) and the Max Planck Institute for the Physics of Complex Systems (Dresden). D.S. thanks DST, India for Project No. SR/S2/JCB-44/2010 for financial support.

<sup>1</sup> L. D'Álessio, Y. Kafri, A. Polkovnikov, M. Rigol, Adv. Phys. **65**, 239 (2016).

<sup>2</sup> J. M. Deutsch, Phys. Rev. A **43**, 2046 (1991).

<sup>3</sup> M. Srednicki, Phys. Rev. E **50**, 888 (1994); J. Phys. A **32**, 1163 (1999).

<sup>4</sup> M. Rigol, V. Dunjko, and M. Olshanii, Nature (London)

**452**, 854 (2008).

<sup>5</sup> A. Lazarides, A. Das, and R. Moessner, Phys. Rev. Lett. **112**, 150401 (2014); Phys. Rev. E **90**, 012110 (2014); P. Ponte, A. Chandran, Z. Papic, and D. A. Abanin, Ann. Phys. (Amsterdam) **353**, 196 (2014); A. Sen, S. Nandy, and K. Sengupta, Phys. Rev. B **94**, 214301 (2016).

- <sup>6</sup> L. D'Álessio and M. Rigol, Phys. Rev. X **4**, 041048 (2014).
- <sup>7</sup> M. Basko, I. L. Aleiner, and B. L. Altshuler, Ann. Phys. **321**, 1126 (2006); V. Oganesyan and D. A. Huse, Phys. Rev. B **75**, 155111 (2007); A. Pal and D. A. Huse, *ibid.* **82**, 174411 (2010); D. A. Huse, R. Nandkishore, V. Oganesyan, A. Pal, and S. L. Sondhi, *ibid.* **88**, 014206 (2013); R. Vosk and E. Altman, Phys. Rev. Lett. **110**, 067204 (2013); M. Serbyn, Z. Papic, and D. A. Abanin, *ibid.* **111**, 127201 (2013); D. A. Huse, R. Nandkishore, and V. Oganesyan, Phys. Rev. B **90**, 174202 (2014); T. Grover, arXiv:1405.1471; M. Serbyn, Z. Papic, and D. A. Abanin, Phys. Rev. X **5**, 041047 (2015); K. Agarwal, S. Gopalakrishnan, M. Knap, M. Müller, and E. Demler, Phys. Rev. Lett. **114**, 160401 (2015); V. Khemani, S. P. Lim, D. N. Sheng, and D. A. Huse, Phys. Rev. X **7**, 021013 (2017).
- <sup>8</sup> E. J. Heller, Phys. Rev. Lett. **53** 1515 (1984); S. Sridhar, *ibid.* **67**, 785 (1991).
- <sup>9</sup> H. Bernien, S. Schwartz, A. Keesling, H. Levine, A. Omran, H. Pichler, S. Choi, A. S. Zibrov, M. Endres, M. Greiner, V. Vuletic, and M. D. Lukin, Nature **551**, 579-584 (2017).
- <sup>10</sup> S. Choi, C. J. Turner, H. Pichler, W. W. Ho, A. A. Michailidis, Z. Papic, M. Serbyn, M. D. Lukin, D. A. Abanin, Phys. Rev. Lett. **122**, 220603 (2019); W. W. Ho, S. Choi, H. Pichler, M. D. Lukin, *ibid.* **122**, 040603 (2019); C. J. Turner, A. A. Michailidis, D. A. Abanin, M. Serbyn, Z. Papic, Nat. Phys. **14** 745 (2018); *ibid.*, Phys. Rev. B **98**, 155134 (2018); C. J. Turner, A. A. Michailidis, D. A. Abanin, M. Serbyn, Z. Papic, arXiv:1905.08564 (unpublished); K. Bull, I. Martin, Z. Papic, arXiv:1903.10491 (unpublished).
- <sup>11</sup> V. Khemani, C.R. Lauman, A. Chandran, Phys. Rev. B **99**, 161101 (2019); S. Maudgalya, N. Regnault, B.A. Bernevig, Phys. Rev. B **98**, 235156 (2018); *ibid.*, arXiv:1906.05292 (unpublished); T. Iadecola, M. Schechter, S. Xu, arXiv:1903.10517; N. Shiraishi, arXiv:1904.05182 (unpublished); M. Schechter, T. Iadecola, arXiv:1906.10131 (unpublished).
- <sup>12</sup> B. Mukherjee, S. Nandy, A. Sen, D. Sen and K. Sengupta, arXiv:1907.08212.
- <sup>13</sup> T. Kitagawa, E. Berg, M. Rudner, and E. Demler, Phys. Rev. B **82**, 235114 (2010); N. H. Lindner, G. Refael, and V. Galitski, Nat. Phys. **7**, 490 (2011); L. Jiang, T. Kitagawa, J. Alicea, A. R. Akhmerov, D. Pekker, G. Refael, J. I. Cirac, E. Demler, M. D. Lukin, and P. Zoller, Phys. Rev. Lett. **106**, 220402 (2011); 2011; T. Kitagawa, T. Oka, A. Brataas, L. Fu, and E. Demler, Phys. Rev. B **84**, 235108 (2011); R. Citro, EG Dalla Torre, L. D'Álessio, A. Polkovnikov, M. Babadi, T. Oka, and E. Demler, Ann. Phys. **393**, 694 (2015); B. Mukherjee, Phys. Rev. B **98**, 235112 (2018).
- <sup>14</sup> L. D. ALESSIO, and A. Polkovnikov, Ann. Phys. **333**, 19 (2013); S. Blanes, F. Casas, J.A. Oteo, and J. Ros, Phys. Rep. **470**, 151 (2009).
- <sup>15</sup> S. Sachdev, K. Sengupta, and S. M. Girvin, Phys. Rev. B **66**, 075128 (2002); S. Pielawa, T. Kitagawa, E. Berg, and S. Sachdev, Phys. Rev. B **83**, 205135 (2011).
- <sup>16</sup> A. Thue, Norske Vidi-densk. Selsk. Skr. I. **7**, 1 (1906); M. Morse, Trans. Am. Math. Soc. **22**, 84 (1921), *ibid.*, M. Morse, Am. J. Math. **43**, 35 (1921).
- <sup>17</sup> S. Nandy, A. Sen, and D. Sen, Phys. Rev. X **7**, 031034 (2017).
- <sup>18</sup> K. Sengupta, S. Powell, and S. Sachdev, Phys. Rev. A **69**, 053616 (2004); M. Kolodrubetz, D. Pekker, B. K. Clark, and K. Sengupta, Phys. Rev. B **85**, 100505 (2012); U. Divakaran and K. Sengupta, Phys. Rev. B **90**, 184303 (2014); P. Fendley, K. Sengupta, and S. Sachdev, Phys. Rev. B **69**, 075106 (2004); R. Samajdar, S. Choi, H. Pichler, M. D. Lukin, and S. Sachdev, Phys. Rev. A **98**, 023614 (2018); R. Ghosh, A. Sen, and K. Sengupta, Phys. Rev. B **97**, 014309 (2018).
- <sup>19</sup> J. Simon, W. S. Bakr, R. Ma, M. E. Tai, P. M. Preiss, and M. Greiner, Nature (London) **472**, 307 (2011); W. Bakr, A. Peng, E. Tai, R. Ma, J. Simon, J. Gillen, S. Foelling, L. Pollet, and M. Greiner, Science **329**, 547 (2010).
- <sup>20</sup> B. Sutherland, Phys. Rev. Lett. **57**, 770 (1986).
- <sup>21</sup> S. Nandy, A. Sen, and D. Sen, Phys. Rev. B **98**, 245144 (2018); Z. Cai, C. Hubig, and U. Schollwck Phys. Rev. B **96**, 054303 (2017).